First direct limit on the 395 keV resonance of the ^{22}Ne(α, γ)^{26}Mg reaction

Eliana Masha[1,2,*] *for the LUNA collaboration*[2]

[1]Università degli studi di Milano and INFN Sezione di Milano
[2]https://luna.lngs.infn.it

Abstract. The ^{22}Ne(α, γ)^{26}Mg reaction (Q = 10614.74 keV) competes with the ^{22}Ne(α, n)^{25}Mg reaction (Q = -478.34 keV) which is the main source of neutrons for the s-process in low-mass Asymptotic Giant Branch and massive stars. The cross sections of these reactions are crucial to fix the cross over temperature at which (α, n) rate exceeds the (α, γ) one. Moreover, the uncertainty on the ^{22}Ne(α, γ)^{26}Mg reaction rate affects also the nucleosynthesis of isotopes between ^{26}Mg and ^{31}P in intermediate-mass stars.
At lower temperatures (T < 300 MK) where the (α, γ) channel is dominant, the rate of the ^{22}Ne(α, γ)^{26}Mg reaction is influenced by several resonances. The present study focuses on the E_α = 395 keV resonance which so far have been studied only indirectly leading to a wide range of possible values for its resonance strength (10^{-15} - 10^{-9} eV).
The experiment has been completed at LUNA using the intense alpha beam of the LUNA 400 kV accelerator and a windowless differential-pumped gas target combined with a high efficiency BGO detector. Experimental details and preliminary results will be shown.

1 Astrophysical motivation and state of the art

The ^{22}Ne(α, γ)^{26}Mg reaction competes with the ^{22}Ne(α, n)^{25}Mg reactions which plays a key role in astrophysics because of its impact on the neutron flux during the s-process. The ^{22}Ne(α, n)^{25}Mg (Q_{value} = -478 keV) reaction is one of the two main neutron sources for the s-process in low-mass Asymptotic Giant Branch (AGB) stars [1] and in massive stars [2]. Its role as a neutron source is affected by the ^{22}Ne(α, γ)^{26}Mg reaction (Q_{value} = 10.6 MeV). This last one can be active during the entire He-burning phase, reducing the amount of the ^{22}Ne before the ^{22}Ne(α, n)^{25}Mg reaction is activated. Therefore, to constrain the role of the ^{22}Ne(α, n)^{25}Mg reaction in the s-process, the rate for both reactions is required. Moreover, recent studies show that the uncertainties of the ^{22}Ne(α, γ)^{26}Mg reaction rate affects also the nucleosynthesis of isotopes between ^{26}Mg and ^{31}P in intermediate-mass AGB stars [3].

The ^{22}Ne(α, γ)^{26}Mg reaction rate at astrophysical temperatures of interest (0.1 GK ≤ T ≤ 0.4 GK) is dominated by several resonances. In particular, the present work is dedicated to the 395 keV (corresponding to the E = 10949 keV excited level of the ^{26}Mg) resonance which has been studied only indirectly. All these studies, lead to a wide range of reported values for its resonance strength (10^{-14} - 10^{-9} eV). Table 1 summarizes the state of the art

*e-mail: eliana.masha@unimi.it

Table 1: Summary of the literature on the E_α = 395 keV resonance strength.

Lower Limit [eV]	Adopted $\omega\gamma[eV]$	Upper Limit [eV]	Reference
1.4×10^{-14}	1.7×10^{-13}	1.6×10^{-12}	Giesen et al. 1993 [4]
-	4.7×10^{-13}	-	Giesen et al. corrected
-	1.4×10^{-13}	1.3×10^{-12}	NACRE 1999 [5]
-	-	3.6×10^{-9}	Iliadis et al. 2010 [6]
-	-	8.7×10^{-15}	Longland et al. 2012 [7]
-	-	3.6×10^{-9}	STARLIB 2013 [8]
-	-	8.7×10^{-14}	Lotay et al. 2019 [9]
-	9.0×10^{-14}		Jayatissa et al. 2020 [10]
-	-	9.0×10^{-14}	Ota et al. 2020 [11]
-	-	8.7×10^{-15}	Adsley et al. 2021 [12]

for the 395 keV resonance and different adopted values for some recent evaluations of the ^{22}Ne$(\alpha,\gamma)^{26}$Mg reaction rate. To reduce this wide range on the resonance strength and to constrain its role in the ^{22}Ne$(\alpha,\gamma)^{26}$Mg reaction rate we have afforded the first direct study of the 395 keV resonance.

2 Experimental setup and data taking

The study of the 395 keV resonance for the ^{22}Ne$(\alpha,\gamma)^{26}$Mg reaction was performed at LUNA (Laboratory for Underground Nuclear Astrophysics), located at Gran Sasso underground laboratories (LNGS). The Gran Sasso rock overburden of about 1400 m (3800 meters of water equivalent), allows the attenuation of the cosmic-ray muon flux by six orders of magnitude and the neutron component by three orders of magnitude compared with the surface laboratories [13–15]. In the region of interest for the ^{22}Ne$(\alpha,\gamma)^{26}$Mg reaction (E_γ= 9998 – 11286 keV) the muon flux is negligible and the main component of the background is due to neutrons. The study of the 394 keV resonance was performed exploiting the gas target beamline combined with a high-efficiency BGO detection system. The data taking was completed in two subsequent campaigns: Campaign I (Summer 2016) and Campaign II (Spring - Summer 2019).

Specific details from Campaign I can be found in [20]. The present work is focused on the data taking and the results obtained in Campaign II. The setup used in Campaign I was mainly the same used in [16]. Same setup was adopted in Campaign II ([17]) except for some improvements which allowed to refine the results of Campaign I. Figure 1 and Figure 2 show the experimental setup adopted in Campaign I and Campaign II, respectively.

The α beam of 399.9 keV laboratory energy and $\sim$ 250 μA coming from the LUNA 400 kV accelerator [18] was delivered to a dedicated target chamber, filled with 1.0 mbar enriched ^{22}Ne (99.9%). The target chamber was partially occupied by the calorimeter which continuously measures the beam intensity. Both the target chamber and the calorimeter were located inside the borehole of the detector which consists of six optically independent BGO crystals. The beam induced-background generated when the beam reaches particular contaminants in different parts of the setup was monitored delivering 399.9 keV α beam on inert Ar gas at 0.468 mbar. Such pressure was selected to assure the same energy loss as that of ^{22}Ne gas at 1 mbar. At this beam energy, the argon gas is expected to be not reactive and therefore allows to identify contaminants in the target chamber which can be source of background for the experiment. A summary of the data taking of Campaign II is given in Table 2. The

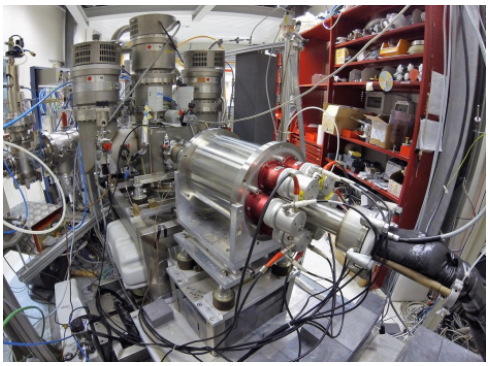

Figure 1: Setup adopted for Campaign I.

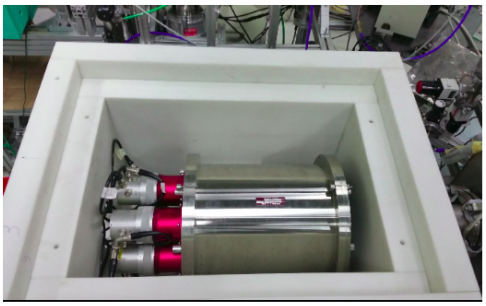

Figure 2: Setup improved for Campaign II.

Table 2: Experimental campaign II. Charge Q, running time t in days and beam energy for on-resonance measurements (α+ ^{22}Ne), beam induced background runs (α+ Ar) and for no-beam background are given.

Charge [C]	t [d]	E_α [keV]	Run type
430.5	23.8	399.9	α+ ^{22}Ne
75.6	7.2	399.9	α+ Ar
	40.1	-	Laboratory background

preliminary analysis of Campaign I [20] showed a slight of 0.4σ excess in the net counting rate. Therefore, to confirm a possible resonance detection further improvements on the setup and detailed study of the background sources were required. In particular, at the energies of interest for the 395 keV resonance, the background in the BGO detector at LUNA was mainly given by neutron-induced effects ([21]). To reduce these effects, a 10 cm thick borated (5%) polyethylene (PE-HMW 500 BOR5 by Profilan Kunstofiwerk) shield surrounded the BGO in Campaign II.

Figure 3 shows the comparison of the laboratory background taken with (Campaign II) and without (Campaign I) shielding. The shielding reduced the count rate in the region of interest for the 334 keV resonance by a factor of 3.27 ±0.3.
The acquisition of the list mode data was done using the MC^2 Analyzer software by CAEN which allows to acquire and save information event by event.
The offline analysis was performed using a software program that was able to process the data after the acquisition and generates two types of spectra: the singles sum spectrum obtained by simply summing the individual histograms by each crystal and the add-back spectrum that sums the energies of all crystals.
The detection efficiency was studied combining the experimental measurements with Monte Carlo simulations (Geant3 and Geant4). The low energy efficiency was measured using the standard radioactive sources (^{7}Be ^{60}Co, ^{88}Y, and ^{137}Cs) in different positions along the beam axis inside the target chamber, while the high energy efficiency was completed using the ^{14}N(p, γ)^{15}O reaction at the 278 keV resonance. The adopted detection efficiency in the region of interest for the ^{22}Ne(α, γ)^{26}Mg was of $\sim$ 40%.

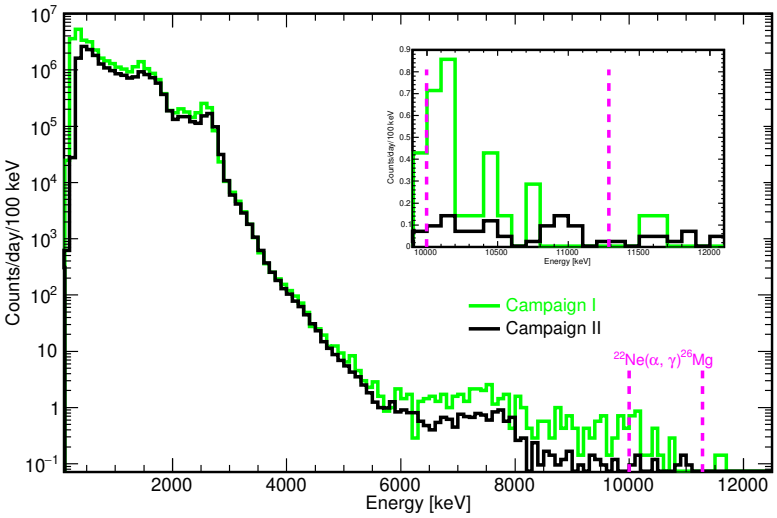

Figure 3: Laboratory background taken during Campaign I (green line) and Campaign II (black line). The dashed magenta lines define the ROI for the 395 keV resonance.

2.1 Results and conclusions

From the analysis of both campaigns no evident signal was detected in the region of interest. The sum of all the corresponding addback spectra for the α + ^{22}Ne runs compared with the

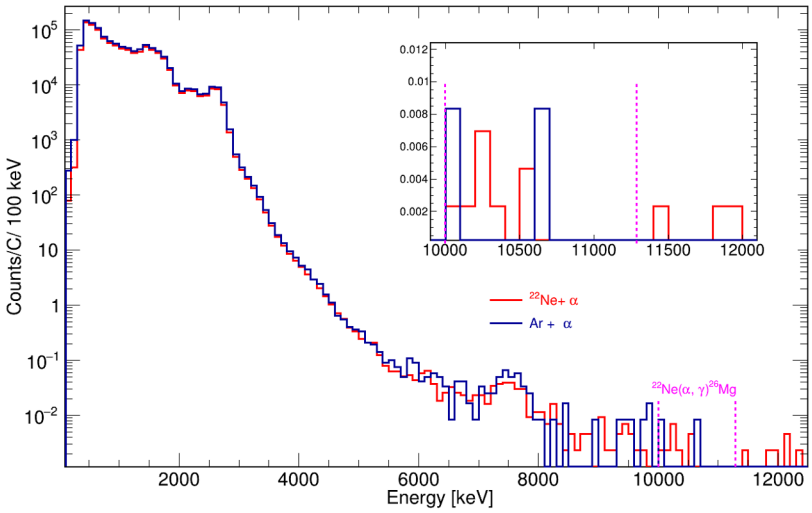

Figure 4: Addback mode spectra. In red the sum of all addback spectra in α+ ^{22}Ne obtained during Campaign II. In blue the sum of the spectra in Ar used for the study of the beam induced background. The dashed magenta lines define the ROI for the 395 keV resonance.

beam-induced background (α + Ar), and a zoom in the identified region of interest are given in Figure 4.

From the present experiment, an upper limit for the 395 keV resonance strength was determined taking into account several corrections due to the use of the gas target and the effects of the beam passing through the gas. The target characterization is given in [16].
The 395 keV resonance is a narrow resonance, total width much larger than the resonance energy. On the other hand, the target thickness in units of keV ($\sim$ 8 keV) is much larger than the total width. Therefore, the connection between the resonance strength $\omega\gamma$ and the experimental yield Y follow the so-called thick-target yield formula.
When the α beam (ΔE_{beam} = 0.1 keV) coming from the accelerator reaches the gas target, the beam broadens due to the energy straggling effects, up to $\sigma E_{straggle}$ = 1.4 keV at the end of the target. Furthermore, the efficiency-corrected density profile deviates from an ideal box shape. The convolution of these two effects introduces a correction factor that takes into account the reduction of the experimental yield due to the finite beam energy width and the target density profile. In the present work, the effect of the energy straggling on the total resonance yield, and hence in the final upper limit result is studied adopting the approach given in [13].
In addition, the interaction with the intense ion beam increases the temperature, and the gas density along the beam path may decrease. This effect, known as the beam heating effect has been studied in different gases and should be taken into account in the energy loss determination. The beam heating correction in neon was studied [22] using the resonance scan technique. The beam heating corrections together with the electron screening effect in the laboratory, which is estimated to be 18% in the adiabatic limit [23] are considered in the determination of the 395 keV resonance upper limit.
The upper limit has been determined by using the Rolke Monte Carlo technique [24]. Taking into account the LUNA result, a new updated ^{22}Ne$(\alpha,\gamma)^{26}$Mg thermonuclear reaction was calculated and its impact on the AGB stars was investigated by studying the abundances of neutron-rich magnesium isotopes in the pulse-driven convective zone. This study was performed by using the COLIBRI code [25] assuming a 5M$_\odot$ AGBs model. The results and their astrophysical impact are under revision and will be published soon.

References

[1] Herwig F. Annual Review of Astronomy and Astrophysics**43** 435 (2005);
[2] Couch R. G. *et al.,* The Astrophysical Journal **190** 95 (1974);
[3] Karakas A. I. *et al.,* The Astrophysical Journal **643** 471 (2006);
[4] Giesen U. *et al.,* Nuclear Physics A **561** 95 (1993);
[5] Angulo C. *et al.,* Nuclear Physics A **656** 3 (1999);
[6] Iliadis C. *et al.,* Nuclear Physics A **841** 31 (2009);
[7] Longland R. *et al.,* Physical Review C **80** 055803 (2009);
[8] Sallaska A. L. *et al.,* The Astrophysical Journal Supplement Series **207** 18 (2013);
[9] Lotay G. *et al.,* The European Physical Journal A **55** 109 (2019);
[10] Jayatissa, G. *et al.,* Phys. Lett. B **802** 135267 (2020),
[11] Ota S. *et al.,* Phys. Lett. B **802** 135256 (2020);
[12] Adsley, P. *et al.,*Physical Review C **103** 015805 (2021);
[13] Bemmerer D. *et al.,*Eur. Phys. J. A**24** 313 (2005);
[14] Caciolli A. *et al.,*Eur. Phys. J. A **34** 179 (2009);
[15] Szucs, T. *et al.,*Eur. Phys. J. A **44** 513 (2010);
[16] Ferraro F. *et al.,* Physical Journal A **54** 44 (2018);

[17] Masha E. EPJ Web of Conferences **227** 02004 (2020);
[18] Formicola A. *et al.,*Nucl. Instr. and Meth. A **507** 609 (2003);
[19] Broggini C. *et al.,* Progress in Particle and Nuclear Physics **98** 55 (2018);
[20] Piatti D. The Study of ^{22}Ne(α, γ)^{26}Mg and ^{6}Li(p, γ)^{7}Be Reactions at LUNA , PhD thesis Padua (2018);
[21] Boeltzig A. *et al.,* Journal of Physics G: Nuclear and Particle Physics **45** 025203 (2018);
[22] Depalo R. The neon-sodium cycle: Study of the ^{22}Ne(p,γ)^{23}Na reaction at astrophysical energies, PhD thesis Padua (2015)
[23] Assenbaum, H. J *et al.,* Zeitschrift für Physik A Atomic Nuclei **327** 4 (1987)
[24] Rolke W., *et al.,* Nucl. Inst. Meth. A **458** 745-758 (2001);
[25] Marigo P., *et al.,* Monthly Notices of the Royal Astronomical Society **434** 488-526 (2013);